arXiv:0807.1025v1 [hep-ex] 7 Jul 2008

EUROPEAN ORGANIZATION FOR NUCLEAR RESEARCH

CERN–PH–EP/2008–010
6 February 2008

Forward $\pi^{\pm}$ production in p–O_2 and p–N_2 interactions at 12 GeV/c

HARP Collaboration

ABSTRACT

Measurements of double-differential charged pion production cross-sections in interactions of 12 GeV/c protons on O_2 and N_2 thin targets are presented in the kinematic range 0.5 GeV/$c \leq p_\pi <$ 8 GeV/c and 50 mrad $\leq \theta_\pi <$ 250 mrad (in the laboratory frame) and are compared with p–C results. For p–N_2 (p–O_2) interactions the analysis is performed using 38576 (7522) reconstructed secondary pions. The analysis uses the beam instrumentation and the forward spectrometer of the HARP experiment at CERN PS. The measured cross-sections have a direct impact on the precise calculation of atmospheric neutrino fluxes and on the improved reliability of extensive air shower simulations by reducing the uncertainties of hadronic interaction models in the low energy range. In particular, the present results allow the common hypothesis that p–C data can be used to predict the p–N_2 and p–O_2 pion production cross-sections to be tested.

Submitted to Astroparticle Physics

M.G. Catanesi, E. Radicioni
Sezione INFN, Bari, Italy
R. Edgecock, M. Ellis[1]
Rutherford Appleton Laboratory, Chilton, Didcot, UK
C. Gößling
Institut für Physik, Universität Dortmund, Germany
S. Bunyatov, A. Krasnoperov, B. Popov[2], V. Tereschenko
Joint Institute for Nuclear Research, JINR Dubna, Russia
E. Di Capua, G. Vidal–Sitjes[3]
Università degli Studi e Sezione INFN, Ferrara, Italy
A. Artamonov[4], S. Giani, S. Gilardoni, P. Gorbunov[4], A. Grant, A. Grossheim[6], A. Ivanchenko[16], V. Ivanchenko[7], A. Kayis-Topaksu[8], J. Panman, I. Papadopoulos, E. Tcherniaev, I. Tsukerman[4], C. Wiebusch[9], P. Zucchelli[5,10]
CERN, Geneva, Switzerland
A. Blondel, S. Borghi[11], M.C. Morone[12], G. Prior[13], R. Schroeter
Section de Physique, Université de Genève, Switzerland
C. Meurer
Institut für Physik, Forschungszentrum Karlsruhe, Germany
U. Gastaldi
Laboratori Nazionali di Legnaro dell' INFN, Legnaro, Italy
G. B. Mills[14]
Los Alamos National Laboratory, Los Alamos, USA
J.S. Graulich[15], G. Grégoire
Institut de Physique Nucléaire, UCL, Louvain-la-Neuve, Belgium
M. Bonesini, F. Ferri
Sezione INFN Milano Bicocca, Milano, Italy
M. Kirsanov
Institute for Nuclear Research, Moscow, Russia
A. Bagulya, V. Grichine, N. Polukhina
P. N. Lebedev Institute of Physics (FIAN), Russian Academy of Sciences, Moscow, Russia
V. Palladino
Università "Federico II" e Sezione INFN, Napoli, Italy
L. Coney[14], D. Schmitz[14]
Columbia University, New York, USA
G. Barr
Nuclear and Astrophysics Laboratory, University of Oxford, UK
F. Bobisut[a,b], D. Gibin[a,b], A. Guglielmi[b], M. Mezzetto[b]
Università degli Studi[a] e Sezione INFN[b], Padova, Italy
J. Dumarchez
LPNHE, Universités de Paris VI et VII, Paris, France
U. Dore
Università "La Sapienza" e Sezione INFN Roma I, Roma, Italy
D. Orestano[c,d], F. Pastore[c,d], A. Tonazzo[c,d], L. Tortora[d]
Università degli Studi[c] e Sezione INFN[d] Roma III, Roma, Italy
C. Booth, L. Howlett
Dept. of Physics, University of Sheffield, UK
M. Bogomilov, D. Kolev, R. Tsenov
Faculty of Physics, St. Kliment Ohridski University, Sofia, Bulgaria
S. Piperov, P. Temnikov
Institute for Nuclear Research and Nuclear Energy, Academy of Sciences, Sofia, Bulgaria
M. Apollonio[17], P. Chimenti, G. Giannini
Università degli Studi e Sezione INFN, Trieste, Italy

J. Burguet–Castell, A. Cervera–Villanueva, J.J. Gómez–Cadenas, J. Martín–Albo, M. Sorel
Instituto de Física Corpuscular, IFIC, CSIC and Universidad de Valencia, Spain

[1]Now at FNAL, Batavia, Illinois, USA.
[2]Also supported by LPNHE, Paris, France.
[3]Now at Imperial College, University of London, UK.
[4]ITEP, Moscow, Russian Federation.
[5]Now at SpinX Technologies, Geneva, Switzerland.
[6]Now at TRIUMF, Vancouver, Canada.
[7]On leave of absence from Ecoanalitica, Moscow State University, Moscow, Russia.
[8]Now at Çukurova University, Adana, Turkey.
[9]Now at III Phys. Inst. B, RWTH Aachen, Aachen, Germany.
[10]On leave of absence from INFN, Sezione di Ferrara, Italy.
[11]Now at CERN, Geneva, Switzerland.
[12]Now at University of Rome Tor Vergata, Italy.
[13]Now at Lawrence Berkeley National Laboratory, Berkeley, California, USA.
[14]MiniBooNE Collaboration.
[15]Now at Section de Physique, Université de Genève, Switzerland, Switzerland.
[16]On leave from Novosibirsk State University, Novosibirsk, Russia.
[17]Now at Nuclear and Astrophysics Laboratory, Oxford University, UK.

1 Introduction

The HARP experiment [1] at the CERN PS was designed to measure hadron yields from a large range of nuclear targets and for incident particle momenta from 1.5 GeV/c to 15 GeV/c. This corresponds to a proton momentum region of great interest for neutrino beams and far from being covered by earlier dedicated hadroproduction experiments [2, 3]. The main motivations are the measurement of pion yields for a quantitative design of the proton driver of a future neutrino factory [4], a substantial improvement in the calculation of the atmospheric neutrino fluxes [5] and the measurement of particle yields as input for the flux calculation of accelerator neutrino experiments [6], such as K2K [7, 8], MiniBooNE [9] and SciBooNE [10].

Measurements of the double-differential cross-section for $\pi^{\pm}$ production at large angles by protons in the momentum range of 3 GeV/c–12.9 GeV/c impinging on different thin 5% nuclear interaction length (λ_{I}) targets have been reported in [11, 12, 13, 14]. These measurements are of special interest for target materials used in conventional accelerator neutrino beams and in neutrino factory designs.

The results on the forward production of π^{+} in p–Al interactions at 12.9 GeV/c and p–Be interactions at 8.9 GeV/c, useful for the understanding of the accelerator neutrino fluxes in the K2K, MiniBooNE and SciBooNE experiments, have been published in references [15, 16].

In this paper we address another of the main motivations of the HARP experiment: the measurement of the yields of positive and negative pions relevant for a precise calculation of the atmospheric neutrino fluxes and improved modeling of extensive air showers. We present measurements of the double-differential cross-section $\mathrm{d}^2\sigma^{\pi}/\mathrm{d}p\mathrm{d}\Omega$ for positive and negative pion production (in the kinematic range of momentum 0.5 GeV/$c \leq p_{\pi} <$ 8 GeV/c and angle 50 mrad $\leq \theta_{\pi} <$ 250 mrad in the laboratory frame) by protons of 12 GeV/c momentum impinging on thin cryogenic N_2 and O_2 targets of 5.5% and 7.5% nuclear interaction length (λ_{I}), respectively. Results for the pion production on a thin carbon target in almost the same kinematic region have already been published in [17]. Some of those results will be shown again in this paper with a different binning for comparison (see Appendix A). These measurements are performed using the forward spectrometer of the HARP detector. Results on the measurement of the double-differential $\pi^{\pm}$ production cross-section in proton–carbon collisions obtained with the HARP large-angle spectrometer (100 MeV/$c \leq p_{\pi} <$ 800 MeV/c and 0.35 rad $\leq \theta_{\pi} <$ 2.15 rad) are presented in a separate article [12].

The existing world data for $\pi^{\pm}$ production on light targets at low beam momentum ($\leq$ 25 GeV/c) are mainly restricted to beryllium targets and with a limited phase space coverage [18, 19, 20, 21, 22, 23]. The work of Eichten et al. [22] has become a widely used standard reference data set. In addition to these data, new results from the E910 Collaboration have been recently published [24].

Carbon is an isoscalar nucleus as nitrogen and oxygen, so the extrapolation to air is the most straightforward. Recently the p–C data at 158 GeV/c provided by the NA49 experiment at CERN SPS in a large acceptance range have become available [25]. Relevant data are expected also from the MIPP experiment at Fermilab [26]. We would like to mention that the NA61 experiment [27] took first p–C data at 30 GeV/c in the autumn of 2007. The foreseen measurements of importance for astroparticle physics are studies of p–C interactions at incoming beam momenta 30 GeV/c, 40 GeV/c, 50 GeV/c and $\pi^{\pm}$–C interactions at 158 GeV/c and 350 GeV/c.

It is more difficult for experiments to study p–O_2 and p–N_2 reactions because cryogenic targets are more complicated to handle. The results presented in this paper are the first for this type of targets in this energy range.

1.1 Experimental apparatus

The HARP experiment [1, 28] makes use of a large-acceptance spectrometer consisting of a forward and large-angle detection system. The HARP detector is shown in Fig. 1. A detailed description of the experimental apparatus can be found in Ref. [28]. The forward spectrometer – based on five modules of large area drift chambers (NDC1-5) [29] and a dipole magnet complemented by a set of detectors for particle identification (PID): a time-of-flight wall (TOFW) [30], a large Cherenkov detector (CHE) and an electromagnetic calorimeter (ECAL) – covers polar angles up to 250 mrad. The muon contamination of the beam is measured with a muon identifier consisting of thick iron absorbers and scintillation counters. The large-angle spectrometer – based on a Time Projection Chamber (TPC) and Resistive Plate Chambers (RPCs) located inside a solenoidal magnet – has a large acceptance in the momentum and angular range for the pions relevant to the production of the muons in a neutrino factory. For the analysis described here only the forward spectrometer and the beam instrumentation are used.

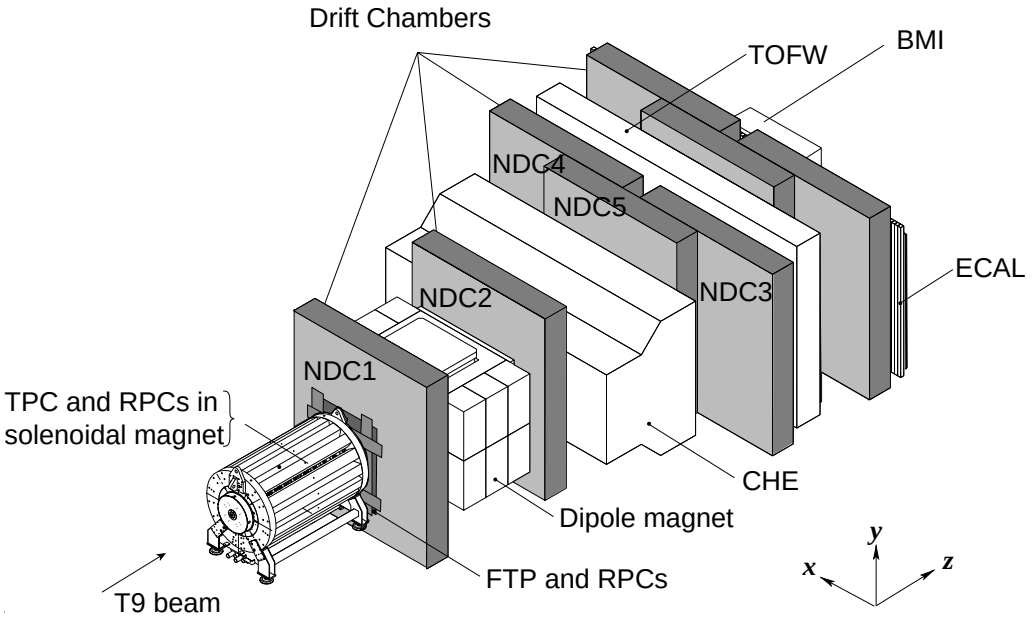

Figure 1: Schematic layout of the HARP detector. The convention for the coordinate system is shown in the lower-right corner.

The HARP experiment, located in the T9 beam of the CERN PS, took data in 2001 and 2002. The momentum definition of the T9 beam is known with a precision of the order of 1% [31].

The target is placed inside the inner field cage (IFC) of the TPC, in an assembly that can be moved in and out of the solenoid magnet. In the cryogenic target setup used for N_2 and O_2, the gas was liquefied by thermal contact with a bath of helium, compressed to 20 bar and then refrigerated to 13 K by adiabatic expansion. The refrigerator system was housed inside a vacuum cryostat (typically 2×10^{-9} bar) ending in a vacuum tube containing the target. The target arm had 6 cm diameter, 250 μm thick mylar beam entrance and exit windows, and the space separating it from the IFC was flushed with nitrogen gas to avoid condensation. The target used for the measurements presented here consisted of a 6 cm long, 3 cm of diameter and 125 μm thick mylar cylinder and a curved downstream nose, for an actual target volume of about 75 cm^3.

The thickness of the target is equivalent to about 5.5% λ_I (4.84 g/cm^2) for N_2 and 7.5% λ_I (6.85 g/cm^2) for O_2.

The cooling causes a contraction of the target, which induces an uncertainty on its thickness of the order of 1%.

This is taken into account in the uncertainty on the number of target nuclei in section 2.3.

A set of four multi-wire proportional chambers (MWPCs) measures the position and direction of the incoming beam particles with an accuracy of ≈1 mm in position and ≈0.2 mrad in angle per projection. A beam time-of-flight system (BTOF) measures the time difference of particles over a 21.4 m path-length. It is made of two identical scintillation hodoscopes, TOFA and TOFB (originally built for the NA52 experiment [32]), which, together with a small target-defining trigger counter (TDS, also used for the trigger), provide particle identification at low energies. This provides separation of pions, kaons and protons up to 5 GeV/c and determines the initial time at the interaction vertex (t_0). The timing resolution of the combined BTOF system is about 70 ps. A system of two N_2-filled Cherenkov detectors (BCA and BCB) is used to tag electrons at low energies and pions at higher energies. The electron and pion tagging efficiency is found to be close to 100%. At the beam energy used for this analysis the Cherenkov counters select all particles lighter than protons, while the BTOF is used to reject ions. A set of trigger detectors completes the beam instrumentation.

The selection of beam protons is performed using the same criteria as described in [15]. A downstream trigger in the forward scintillator trigger plane (FTP) was required to record the event, accepting only tracks with a trajectory outside the central hole (60 mm) which allows beam particles to pass.

The length of the accelerator spill is 400 ms with a typical intensity of 15 000 beam particles per spill. The average number of events recorded by the data acquisition ranges from 300 to 350 per spill.

The absolute normalization of the number of incident protons was performed using 'incident-proton' triggers. These are triggers where the same selection on the beam particle was applied but no selection on the interaction was performed. The rate of this trigger was down-scaled by a factor 64.

2 Data Analysis

2.1 Event and particle selection

A detailed description of the experimental techniques used for data analysis in the HARP forward spectrometer can be found in Ref. [15, 33].

With respect to our first paper on pion production in p–Al interactions [15], a number of improvements to the analysis techniques and detector simulation have been made. The most important improvements introduced in this analysis compared with the one presented in Ref. [15] are:

- An increase of the track reconstruction efficiency;
- Better understanding of the momentum scale and resolution of the detector, based on data, which was then used to tune the simulation;
- New particle identification hit selection algorithms both in the TOFW and in the CHE resulting in much reduced background and negligible efficiency losses. In the kinematic range of the current analysis the pion identification efficiency is about 98%, while the background from mis-identified protons is well below 1%;
- Significant increases in Monte Carlo production have also reduced uncertainties from Monte Carlo statistics and allowed studies which have reduced certain systematics.

Further details of these improved analysis techniques can be found in [16, 17]. For the cryogenic targets, dedicated, high statistics Monte Carlo data were produced using an accurate description of the target geometry.

At the first stage of the analysis a beam particle type is selected using the beam time of flight system (TOF-A, TOF-B) and the Cherenkov counters (BCA, BCB) as described in section 1.1. A value of the pulseheight

Table 1: Total number of events and selected pions used in the carbon, nitrogen and oxygen thin target analysis at 12 GeV/c, and the number of protons on target as calculated from the pre-scaled trigger count.

Data set	C	N_2	O_2
Total DAQ events	1062429	1375780	246153
Acc. beam protons forward interactions	4375230	5250240	840256
π^- **selected with PID**	8179	14828	2817
π^+ **selected with PID**	13530	23748	4705

consistent with the pedestal in both beam Cherenkov detectors rejects electrons, pions and kaons. The beam TOF system is used to reject ions, such as deuterons, but at 12 GeV/c is not used to separate protons from pions. However, we require time measurements in TOF-A, TOF-B and/or TDS to be present which are needed for calculating the arrival time of the beam proton at the target.

The purity of the proton beam is better than 99%, with the main background formed by kaons estimated to be 0.5%. This contamination is neglected in the analysis.

Secondary track selection criteria, described in [17], are optimized to ensure the quality of momentum reconstruction and a clean time-of-flight measurement while maintaining a high reconstruction efficiency.

The background induced by interactions of beam particles in the materials outside the target is measured by taking data without a target in the target holder ("empty target data"). These data are subject to the same event and track selection criteria as the standard data sets.

To take into account this background the number of particles of the observed type (π^+, π^-) in the "empty target data" are subtracted bin-by-bin (momentum and angular bins) from the number of particles of the same type. The uncertainty induced by this method is discussed in section 2.3 and labeled "empty target subtraction". The event statistics is summarised in Table 1.

2.2 Cross-section calculation

The cross-section is calculated as follows

$$\frac{d^2\sigma^\alpha}{dpd\Omega}(p_i,\theta_j) \;=\; \frac{A}{N_A\rho t}\cdot\frac{1}{N_{\rm pot}}\cdot\frac{1}{\Delta p_i\Delta\Omega_j}\cdot\sum_{p'_i,\theta'_j,\alpha'}\mathcal{M}^{\rm cor}_{p_i\theta_j\alpha p'_i\theta'_j\alpha'}\cdot N^{\alpha'}(p'_i,\theta'_j)\;, \tag{1}$$

where

- $\frac{d^2\sigma^\alpha}{dpd\Omega}(p_i,\theta_j)$ is the cross-section in mb/(GeV/c sr) for the particle type α (p, π^+or π^-) for each true momentum and angle bin (p_i,θ_j) covered in this analysis;
- $N^{\alpha'}(p'_i,\theta'_j)$ is the number of particles of type α in bins of reconstructed momentum p'_i and angle θ'_j in the raw data;
- $\mathcal{M}^{\rm cor}_{p\theta\alpha p'\theta'\alpha'}$ is the correction matrix which accounts for efficiency and resolution of the detector;
- $\frac{A}{N_A\rho t}$, $\frac{1}{N_{\rm pot}}$ and $\frac{1}{\Delta p_i\Delta\Omega_j}$ are normalization factors, namely:
  $\frac{N_A\rho t}{A}$ is the number of target nuclei per unit area [1)];
  $N_{\rm pot}$ is the number of incident beam particles on target (particles on target);
  Δp_i and $\Delta\Omega_j$ are the bin sizes in momentum and solid angle, respectively [2)].

[1)] A - atomic mass, N_A - Avogadro number, ρ - target density and t - target thickness
[2)] $\Delta p_i = p_i^{\rm max} - p_i^{\rm min}, \quad \Delta\Omega_j = 2\pi(\cos(\theta_j^{\rm min}) - \cos(\theta_j^{\rm max}))$

We do not make a correction for the attenuation of the proton beam in the target, so that strictly speaking the cross-sections are valid for a $\lambda_{\mathrm{I}} = 5.5\%$ (7.5%) N_2 (O_2) target.

The calculation of the correction matrix $M^{\mathrm{cor}}_{p_i\theta_j\alpha p'_i\theta'_j\alpha'}$ is a rather difficult task. Various techniques are described in the literature to obtain this matrix. As discussed in Ref. [15] for the p-Al analysis of HARP data at 12.9 GeV/c, two complementary analyses have been performed to cross-check internal consistency and possible biases in the respective procedures. A comparison of both analyses shows that the results are consistent within the overall systematic error [15].

In the first method – called "Atlantic" in [15] – the correction matrix $M^{\mathrm{cor}}_{p_i\theta_j\alpha p'_i\theta'_j\alpha'}$ is decomposed into distinct independent contributions, which are computed mostly using the data themselves. The second method – called "UFO" in [15] – is the unfolding method introduced by D'Agostini [34]. It is based on the Bayesian unfolding technique. In this case a simultaneous (three dimensional) unfolding of momentum p, angle θ and particle type α is performed. The correction matrix is computed using a Monte Carlo simulation. This method has been used in the recent HARP publications [11, 12, 13] and it is also applied in the analysis described here (see [17, 36] for additional information).

The Monte Carlo simulation of the HARP setup is based on GEANT4 [37]. The detector materials are accurately described in this simulation as well as the relevant features of the detector response and the digitization process. All relevant physics processes are considered, including multiple scattering, energy loss, absorption and re-interactions. The simulation is independent of the beam particle type because it only generates for each event exactly one secondary particle of a specific particle type inside the target material and propagates it through the complete detector. A small difference (at the few percent level) is observed between the efficiency calculated for events simulated with the single-particle Monte Carlo and with a simulation using a multi-particle hadron-production model. A similar difference is seen between the single-particle Monte Carlo and the efficiencies measured directly from the data. A momentum-dependent correction factor determined using the efficiency measured with the data is applied to take this into account. The track reconstruction used in this analysis and the simulation are identical to the ones used for the π^+ production in p-Be collisions [16]. A detailed description of the corrections and their magnitude can be found there.

The reconstruction efficiency (inside the geometrical acceptance) is larger than 95% above 1.5 GeV/c and drops to 80% at 0.5 GeV/c. The requirement of a match with a TOFW hit has an efficiency between 90% and 95% independent of momentum. The electron veto rejects about 1% of the pions and protons below 3 GeV/c with a remaining background of less than 0.5%. Below Cherenkov threshold the TOFW separates pions and protons with negligible background and an efficiency of ≈98% for pions. Above Cherenkov threshold the efficiency for pions is greater than 99% with only 1.5% of the protons mis-identified as a pion. The kaon background in the pion spectra is smaller than 1%.

The absorption and decay of particles is simulated by the Monte Carlo. The generated single particle can re-interact and produce background particles by hadronic or electromagnetic processes, thus giving rise to tracks in the dipole spectrometer. In such cases also the additional measurements are entered into the migration matrix thereby taking into account the combined effect of the generated particle and any secondaries it creates. The absorption correction is on average 20%, approximately independent of momentum. Uncertainties in the absorption of secondaries in the dipole spectrometer material are taken into account by a variation of 10% of this effect in the simulation. The effect of pion decay is treated in the same way as the absorption and is 20% at 500 MeV/c and negligible at 3 GeV/c.

The uncertainty in the production of background due to tertiary particles is larger. The average correction is ≈10% and up to 20% at 1 GeV/c. The correction includes reinteractions in the detector material as well as a small component coming from reinteractions in the target. The validity of the generators used in the simulation

was checked by an analysis of HARP data with incoming protons, and charged pions on aluminium and carbon targets at lower momenta (3 GeV/c and 5 GeV/c). A 30% variation of the secondary production was applied. The average empty-target subtraction amounts to ≈20%.

Owing to the redundancy of the tracking system downstream of the target the detection efficiency is very robust under the usual variations of the detector performance during the long data taking periods. Since the momentum is reconstructed without making use of the upstream drift chamber module (which is more sensitive in its performance to the beam intensity) the reconstruction efficiency is uniquely determined by the downstream system. No variation of the overall efficiency has been observed. The performance of the TOFW and CHE system have been monitored to be constant for the data taking periods used in this analysis. The calibration of the detectors was performed on a day-by-day basis.

2.3 Error estimation

The total statistical error of the corrected data is composed of the statistical error of the raw data and of the statistical error of the unfolding procedure, as the unfolding matrix is obtained from the data themselves, thus contributing also to the statistical error. The statistical error provided by the unfolding program is equivalent to the propagated statistical error of the raw data. In order to calculate the statistical error of the unfolding procedure a separate analysis is applied, as described in [17, 38]. Its conclusion is that the statistical error provided by the unfolding procedure has to be multiplied globally by a factor of 2, which is done for the analyses described here. This factor is somewhat dependent on the shape of the distributions. For example a value 1.7 was found for the analysis reported in Ref. [11].

Different types of sources induce systematic errors for the analysis described here: track yield corrections ($\sim 5\%$), particle identification ($\sim 0.1\%$), momentum and angular reconstruction ($\sim 0.5\%$) [3)]. The strategy to calculate these systematic errors and the different methods used for their evaluation are described in [17]. An additional source of error is due to misidentified secondary kaons, which are not considered in the particle identification method used for this analysis and are subtracted on the basis of a Monte Carlo simulation, as in [17]. No explicit correction is made for pions coming from decays of other particles created in the target, as they give a very small contribution according to the selection criteria applied in the analysis.

As a result of these systematic error studies, each error source can be represented by a covariance matrix. The sum of these matrices describes the total systematic error, as explained in [17].

On average the total integrated systematic error is around $5-6\%$, with a differential bin to bin systematic error of the order of $10-11\%$, to be compared with a statistical integrated (bin-to-bin differential) error of $\sim 2-3\%$ ($\sim 10-13\%$). Systematic and statistical errors are roughly of the same order.

The overall normalization of the results is calculated relative to the number of incident beam particles accepted by the selection. The uncertainty is 2% for incident protons. The contraction of the target with cooling induces an additional systematic error of 1% on the N_2 and O_2 data.

3 Results

In Figure 2, the measured π^+ and π^- spectra in p–N_2 and p–O_2 interactions at 12 GeV/c are compared to an empirical prametrization, developed by Sanford and Wang [39] to describe the production cross-sections of mesons in proton-nucleus interactions. The parameters fitted to our p–C data at 12 GeV/c in [17] have been

[3)] The quoted error in parenthesis refers to fractional error of the integrated cross-section in the kinematic range covered by the HARP experiment

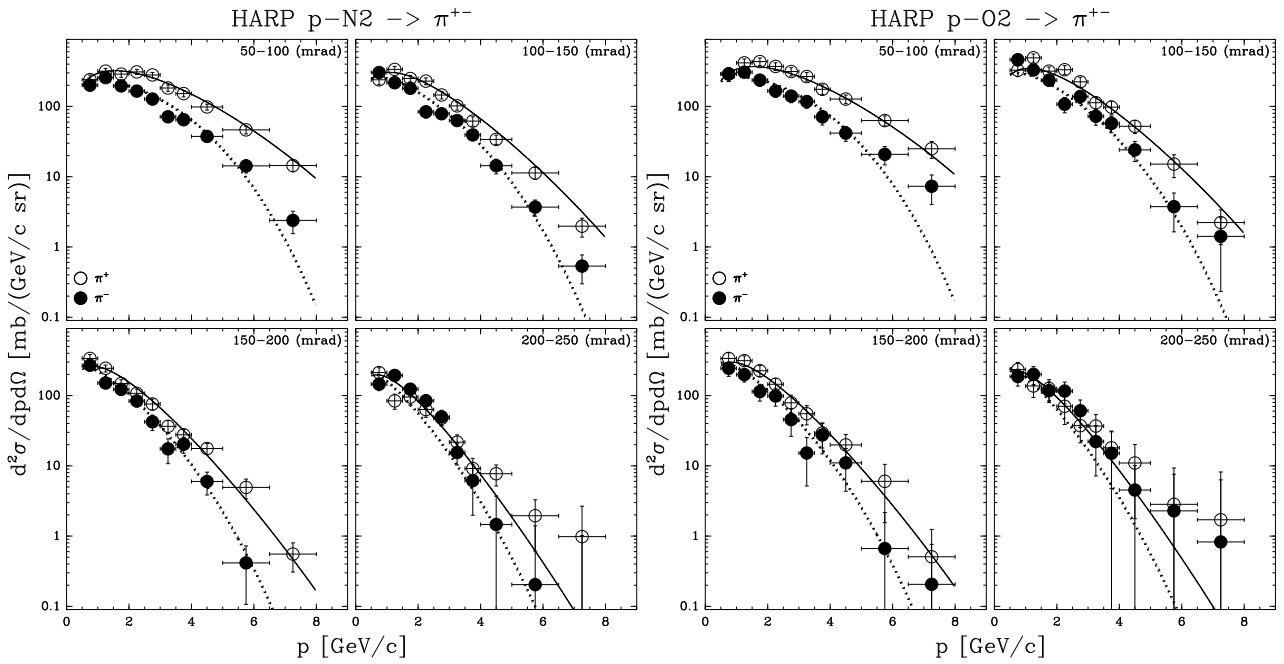

Figure 2: Measurement of the double-differential production cross-section of positive (open circles) and negative (filled circles) pions from 12 GeV/c protons on N_2 (left) and O_2 (right) as a function of pion momentum, p, in bins of pion angle, θ, in the laboratory frame. The curves show the Sanford-Wang parametrization with the parameters given in Ref. [17] (solid line for π^+ and dashed line for π^-), computed for the central value of each angular bin. In the top right corner of each plot the covered angular range is shown in mrad.

used and only a constant overall rescaling factor accounting for the target atomic mass has been applied. One can observe that the shape and normalization obtained using the carbon data predict quite well the nitrogen and oxygen data. This point will be made more clear when the N_2/C and O_2/C ratios are taken. The shapes of the momentum spectra are similar for secondary π^+ and π^- , as well as for different data sets, where only a different normalisation factor can be noticed because of the different nuclear masses of the target nuclei. The conclusions drawn in [17] appear to be confirmed for the data sets presented here: the parametrization provides an approximate description of the main features, but is not able to describe the data well in some regions of kinematic space, particularly at high momenta and at large angles.

The central values and square-root of the diagonal elements of the covariance matrix are listed in Tables 2 and 3.

The kinematic range of the measurements covers the momentum region from 0.5 GeV/c to 8.0 GeV/c (subdivided into 10 intervals) and the angular range from 0.05 rad to 0.25 rad (subdivided into 4 intervals). The error bars correspond to the combined statistical and systematic errors as described in section 2.3. The overall normalization error of 2% for the normalization of incident protons and of 1% for the target size variation are not shown.

The pion production ratios N_2/C and O_2/C are presented in Figs. 3-4 and are compared to GEANT4 Monte Carlo predictions. As noted before, the difference between the target materials is justified by an overall normalisation factor taking into account the different nuclear masses of the target materials. The various models (see [40] for details) do predict the ratio of cross-sections accurately, with very little spread between them. This conclusion is different when the absolute predictions models are compared with the measured cross-sections as shown in Ref. [17].

Table 2: HARP results for the double-differential π^+ and π^- production cross-section in the laboratory system, $d^2\sigma^\pi/(dpd\Omega)$, for p–$N_2$ interactions at 12 GeV/c. Each row refers to a different ($p_{\rm min} \le p < p_{\rm max}, \theta_{\rm min} \le \theta < \theta_{\rm max}$) bin, where p and θ are the pion momentum and polar angle, respectively. The central value as well as the square-root of the diagonal elements of the covariance matrix are given.

$\theta_{\rm min}$ (rad)	θmax (rad)	$p_{\rm min}$ (GeV/c)	$p$max (GeV/c)	$d^2\sigma^{\pi^+}/(dpd\Omega)$ (mb/(GeV/c sr))	$d^2\sigma^{\pi^-}/(dpd\Omega)$ (mb/(GeV/c sr))
0.05	0.10	0.50	1.00	240.5 ± 39.9	200.7 ± 33.7
		1.00	1.50	318.1 ± 29.0	256.9 ± 27.9
		1.50	2.00	288.2 ± 28.1	195.9 ± 23.2
		2.00	2.50	310.5 ± 26.3	165.3 ± 18.0
		2.50	3.00	280.6 ± 23.9	127.4 ± 14.8
		3.00	3.50	183.0 ± 18.9	71.2 ± 10.1
		3.50	4.00	152.3 ± 15.6	64.7 ± 8.8
		4.00	5.00	98.3 ± 9.5	37.5 ± 5.6
		5.00	6.50	46.4 ± 5.8	14.3 ± 3.0
		6.50	8.00	14.4 ± 2.7	2.4 ± 0.8
0.10	0.15	0.50	1.00	239.5 ± 35.5	304.3 ± 42.8
		1.00	1.50	336.9 ± 34.7	217.3 ± 24.5
		1.50	2.00	250.0 ± 27.2	180.8 ± 20.9
		2.00	2.50	229.3 ± 25.6	83.9 ± 15.4
		2.50	3.00	145.3 ± 17.5	78.7 ± 11.9
		3.00	3.50	101.8 ± 13.4	63.0 ± 8.6
		3.50	4.00	61.9 ± 9.6	39.3 ± 6.5
		4.00	5.00	33.9 ± 5.1	14.3 ± 3.4
		5.00	6.50	11.3 ± 2.2	3.7 ± 1.0
		6.50	8.00	2.0 ± 0.6	0.5 ± 0.2
0.15	0.20	0.50	1.00	337.6 ± 45.5	269.8 ± 40.0
		1.00	1.50	244.4 ± 27.8	151.1 ± 21.8
		1.50	2.00	148.6 ± 19.3	122.4 ± 18.7
		2.00	2.50	107.4 ± 15.8	83.7 ± 14.7
		2.50	3.00	75.8 ± 13.6	42.3 ± 10.5
		3.00	3.50	36.5 ± 7.7	17.5 ± 6.7
		3.50	4.00	27.7 ± 5.2	20.3 ± 5.2
		4.00	5.00	17.6 ± 3.1	6.0 ± 2.1
		5.00	6.50	4.9 ± 1.5	0.4 ± 0.3
		6.50	8.00	0.6 ± 0.2	-
0.20	0.25	0.50	1.00	212.6 ± 36.0	145.5 ± 28.0
		1.00	1.50	84.1 ± 20.3	193.4 ± 34.2
		1.50	2.00	95.4 ± 22.3	123.2 ± 25.2
		2.00	2.50	63.2 ± 14.2	84.4 ± 18.5
		2.50	3.00	47.6 ± 10.9	49.8 ± 11.8
		3.00	3.50	21.7 ± 5.9	15.5 ± 5.2
		3.50	4.00	9.2 ± 3.6	6.2 ± 4.2
		4.00	5.00	7.7 ± 2.6	1.5 ± 2.2
		5.00	6.50	1.9 ± 1.3	-
		6.50	8.00	-	-

Table 3: HARP results for the double-differential π^+ and π^- production cross-section in the laboratory system, $d^2\sigma^\pi/(dpd\Omega)$, for p–$O_2$ interactions at 12 GeV/c. Each row refers to a different ($p_{\rm min} \le p < p_{\rm max}, \theta_{\rm min} \le \theta < \theta_{\rm max}$) bin, where p and θ are the pion momentum and polar angle, respectively. The central value as well as the square-root of the diagonal elements of the covariance matrix are given.

$\theta_{\rm min}$ (rad)	θmax (rad)	$p_{\rm min}$ (GeV/c)	$p$max (GeV/c)	$d^2\sigma^{\pi^+}/(dpd\Omega)$ (mb/(GeV/c sr))	$d^2\sigma^{\pi^-}/(dpd\Omega)$ (mb/(GeV/c sr))
0.05	0.10	0.50	1.00	290.3 ± 63.9	290.6 ± 63.3
		1.00	1.50	417.5 ± 56.5	307.7 ± 49.4
		1.50	2.00	435.2 ± 53.9	236.9 ± 41.2
		2.00	2.50	371.4 ± 47.3	166.1 ± 31.4
		2.50	3.00	313.9 ± 42.0	140.5 ± 27.3
		3.00	3.50	266.2 ± 36.9	117.5 ± 23.3
		3.50	4.00	175.3 ± 27.1	71.1 ± 16.7
		4.00	5.00	127.4 ± 18.1	41.7 ± 9.9
		5.00	6.50	63.0 ± 10.3	20.8 ± 6.1
		6.50	8.00	25.0 ± 6.8	7.3 ± 3.3
0.10	0.15	0.50	1.00	327.5 ± 62.5	462.9 ± 85.0
		1.00	1.50	492.2 ± 65.7	330.2 ± 50.0
		1.50	2.00	317.9 ± 46.3	235.9 ± 40.6
		2.00	2.50	332.7 ± 48.5	107.5 ± 26.4
		2.50	3.00	224.1 ± 36.6	138.4 ± 28.8
		3.00	3.50	113.0 ± 21.9	72.6 ± 18.5
		3.50	4.00	97.8 ± 21.7	57.4 ± 15.3
		4.00	5.00	52.2 ± 10.9	24.1 ± 7.6
		5.00	6.50	15.1 ± 5.4	3.7 ± 2.1
		6.50	8.00	2.2 ± 1.1	1.4 ± 1.2
0.15	0.20	0.50	1.00	337.5 ± 69.6	244.2 ± 56.7
		1.00	1.50	313.5 ± 52.3	198.7 ± 42.9
		1.50	2.00	225.6 ± 40.9	113.9 ± 30.5
		2.00	2.50	144.9 ± 30.4	98.7 ± 28.0
		2.50	3.00	78.8 ± 22.3	45.5 ± 19.3
		3.00	3.50	55.2 ± 16.9	15.2 ± 10.0
		3.50	4.00	29.3 ± 11.4	27.5 ± 12.7
		4.00	5.00	19.8 ± 8.0	11.0 ± 6.7
		5.00	6.50	6.0 ± 4.5	-
		6.50	8.00	-	-
0.20	0.25	0.50	1.00	235.0 ± 59.7	186.7 ± 50.2
		1.00	1.50	137.0 ± 43.4	200.3 ± 58.2
		1.50	2.00	126.2 ± 42.0	117.5 ± 38.2
		2.00	2.50	70.2 ± 31.5	115.8 ± 39.6
		2.50	3.00	37.3 ± 16.1	60.8 ± 25.7
		3.00	3.50	36.8 ± 16.7	22.1 ± 15.0
		3.50	4.00	18.0 ± 13.2	15.1 ± 15.3
		4.00	5.00	11.0 ± 9.2	4.5 ± 5.5
		5.00	6.50	2.8 ± 4.8	-
		6.50	8.00	-	-

4 Summary and conclusions

The results reported in this article may contribute to the precise calculations of atmospheric neutrino fluxes and to the improvement of our understanding of extensive air showers simulations and hadronic interactions at low

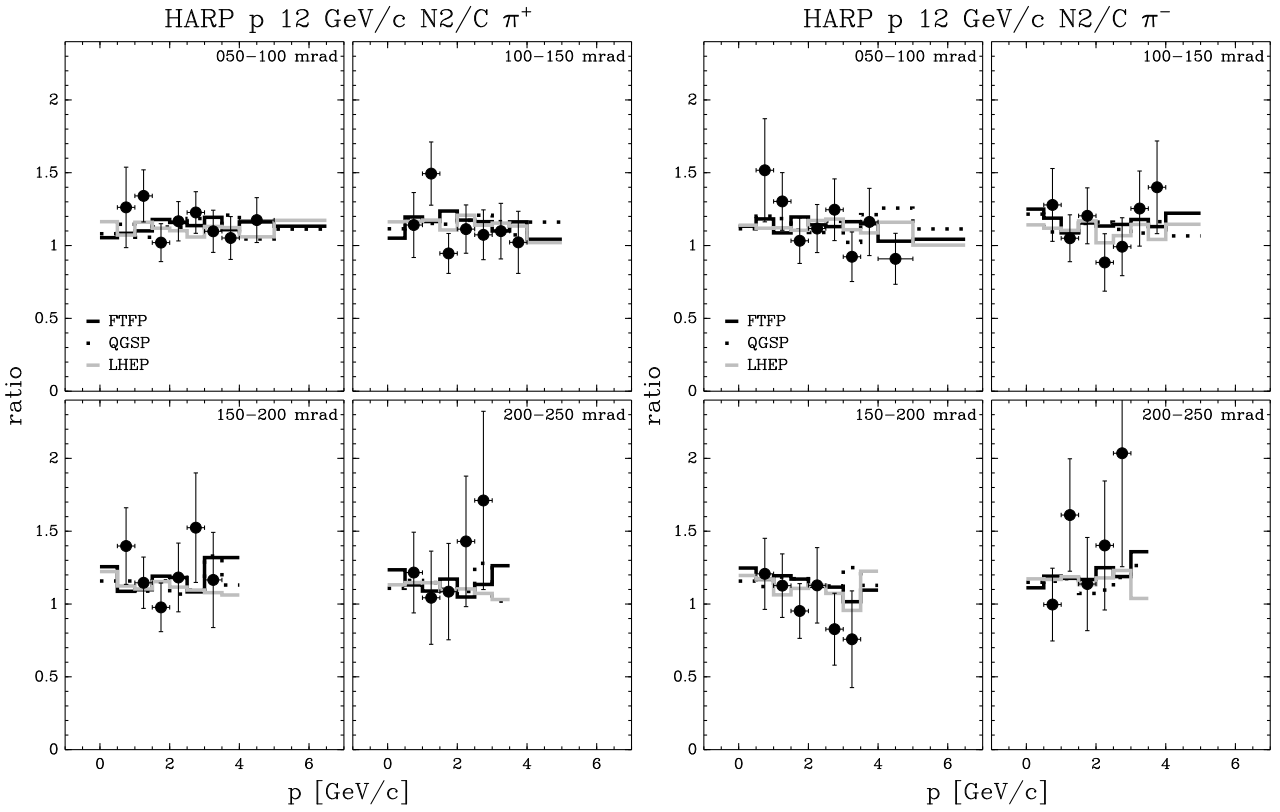

Figure 3: p–N_2 to p–C production ratio for π^+(left panel) and π^-(right panel) at 12 GeV/c, compared with GEANT4 simulation predictions using different models. In the top right corner of each plot the covered angular range is shown in mrad. Only statistical errors are used, since most systematic ones cancel.

energies. A detailed study of the role of hadronic interactions for production of muons in extensive air showers, which are one of the main ingredients to infer the mass and the energy of the primary cosmic ray particle, is shown in reference [35].

In this paper we presented measurements of the double-differential production cross-section of positive and negative pions in the collisions of 12 GeV/c protons with thin nitrogen and oxygen targets. The data were reported in bins of pion momentum and angle in the kinematic range 0.5 GeV/$c \leq p_\pi <$ 8 GeV/c and 0.05 rad $\leq \theta_\pi <$ 0.25 rad in the laboratory frame. A detailed error analysis has been performed yielding total bin-to-bin differential errors (statistical and systematic) of about 15%, an overall normalization error of 2% and additional 1% for the target size variation. We should stress that the HARP data are the first measurements with cryogenic targets in this kinematic region with good precision.

Simulations predict that collisions of protons with a carbon target are very similar to proton interactions with air (see e.g. [36]). That explains why these datasets can be used for tuning models needed in astroparticle physics simulations. Our measurements on p–N_2 and p–O_2 confirm these predictions.

5 Acknowledgments

We gratefully acknowledge the help and support of the PS beam staff and of the numerous technical collaborators who contributed to the detector design, construction, commissioning and operation. In particular, we would like to thank G. Barichello, R. Brocard, K. Burin, V. Carassiti, F. Chignoli, D. Conventi, G. Decreuse, M. Delattre, C. Detraz, A. Domeniconi, M. Dwuznik, F. Evangelisti, B. Friend, A. Iaciofano, I. Krasin, D. Lacroix,

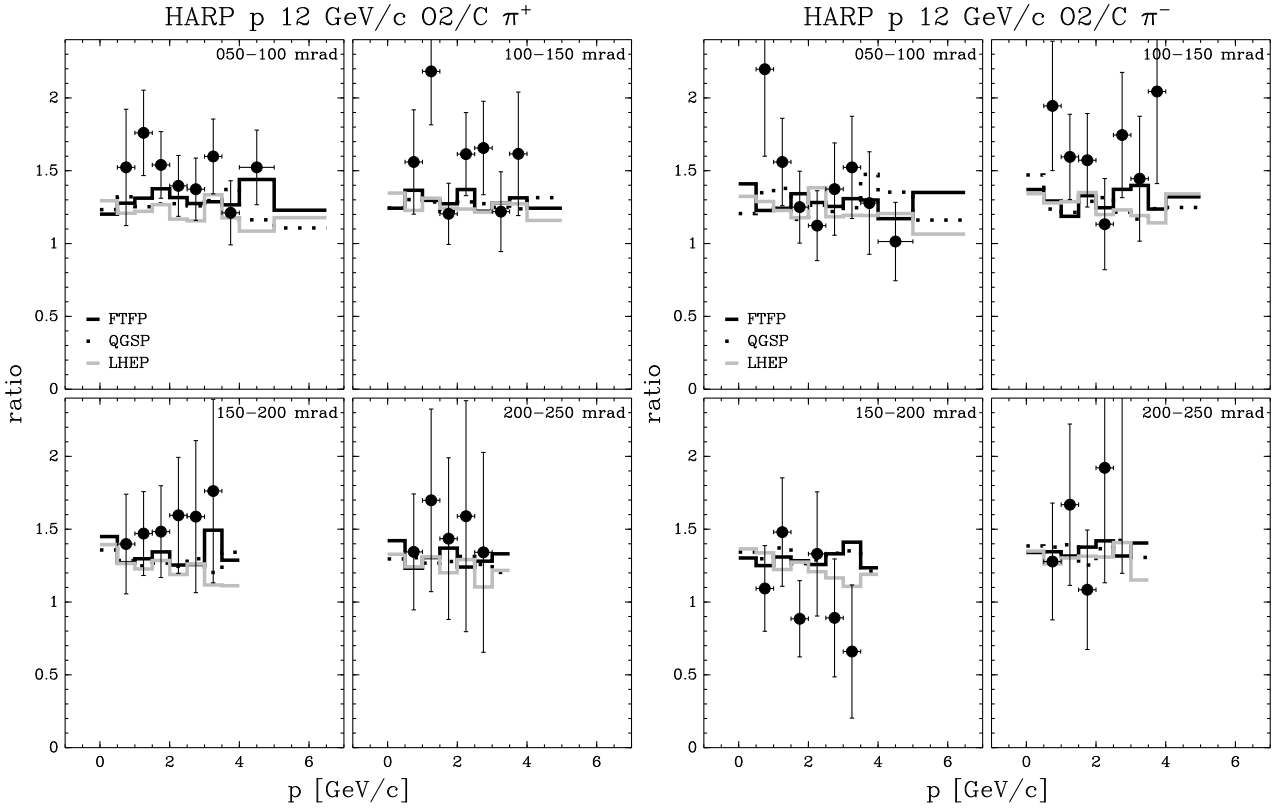

Figure 4: p–O_2 to p–C production ratio for π^+(left panel) and π^-(right panel) at 12 GeV/c, compared with GEANT4 simulation predictions using different models. In the top right corner of each plot the covered angular range is shown in mrad. Only statistical errors are used, since most systematic ones cancel.

J.-C. Legrand, M. Lobello, M. Lollo, J. Loquet, F. Marinilli, R. Mazza, J. Mulon, L. Musa, R. Nicholson, A. Pepato, P. Petev, X. Pons, I. Rusinov, M. Scandurra, E. Usenko, R. van der Vlugt, for their support in the construction of the detector and P. Dini for his contribution to MonteCarlo production. The collaboration acknowledges the major contributions and advice of M. Baldo-Ceolin, L. Linssen, M.T. Muciaccia and A. Pullia during the construction of the experiment. The collaboration is indebted to V. Ableev, F. Bergsma, P. Binko, E. Boter, M. Calvi, C. Cavion, M. Chizov, A. Chukanov, A. DeSanto, A. DeMin, M. Doucet, D. Düllmann, V. Ermilova, W. Flegel, Y. Hayato, A. Ichikawa, O. Klimov, T. Kobayashi, D. Kustov, M. Laveder, M. Mass, H. Meinhard, A. Menegolli, T. Nakaya, K. Nishikawa, M. Paganoni, F. Paleari, M. Pasquali, M. Placentino, V. Serdiouk, S. Simone, P.J. Soler, S. Troquereau, S. Ueda, A. Valassi and R. Veenhof for their contributions to the experiment.

We acknowledge the contributions of V. Ammosov, G. Chelkov, D. Dedovich, F. Dydak, M. Gostkin, A. Guskov, D. Khartchenko, V. Koreshev, Z. Kroumchtein, I. Nefedov, A. Semak, J. Wotschack, V. Zaets and A. Zhemchugov to the work described in this paper.

The experiment was made possible by grants from the Institut Interuniversitaire des Sciences Nucléaires and the Interuniversitair Instituut voor Kernwetenschappen (Belgium), Ministerio de Educacion y Ciencia, Grant FPA2003-06921-c02-02 and Generalitat Valenciana, grant GV00-054-1, CERN (Geneva, Switzerland), the German Bundesministerium für Bildung und Forschung (Germany), the Istituto Nazionale di Fisica Nucleare (Italy), INR RAS (Moscow) and the Particle Physics and Astronomy Research Council (UK). We gratefully acknowledge their support.

References

[1] M. G. Catanesi *et al.*, HARP Collaboration, "Proposal to study hadron production for the neutrino factory and for the atmospheric neutrino flux", CERN-SPSC/99-35 (1999).

[2] G. Ambrosini *et al.* [NA56 Collaboration], Eur. Phys. J. C **10** (1999) 605;
G. Ambrosini *et al.* [NA56 Collaboration], Phys. Lett. B **420** (1998) 225;
G. Ambrosini *et al.* [NA56 Collaboration], Phys. Lett. B **425** (1998) 208.

[3] H.W. Atherton, CERN 80-07, August 1980.

[4] M. Apollonio *et al.*, "Oscillation Physics with a Neutrino Factory", CERN TH2002-208, [arXiv:hep-ph/0210192];
A. Baldini *et al.*, BENE Steering Group, CERN-2006-005;
A. Blondel *et al.*, CERN-2004-002, ECFA/04/230.

[5] M. Honda, T. Kajita, K. Kasahara and S. Midorikawa, Phys. Rev. D **70** (2004) 043008; Phys. Rev. D **75** (2007) 043005 [arXiv:astro-ph/0611201].
M. Honda, T. Kajita, K. Kasahara, S. Midorikawa and T. Sanuki, Phys. Rev. D **75** (2007) 043006 [arXiv:astro-ph/0611418].
G. D. Barr, T. K. Gaisser, P. Lipari, S. Robbins and T. Stanev, Phys. Rev. D **70** (2004) 023006.
G. Battistoni, A. Ferrari, T. Montaruli and P. R. Sala, [arXiv:hep-ph/0305208]
G. Battistoni, A. Ferrari, T. Montaruli and P. R. Sala, Astropart. Phys. **19** (2003) 269 [Erratum-ibid. **19** (2003) 291]
G. Battistoni, A. Ferrari, P. Lipari, T. Montaruli, P. R. Sala and T. Rancati, Astropart. Phys. **12** (2000) 315

[6] M. Bonesini and A. Guglielmi, Phys. Rep. 433 (2006) 66.

[7] E. Aliu *et al.* [K2K Collaboration], "Evidence for muon neutrino oscillation in an accelerator-based experiment," Phys. Rev. Lett. **94** (2005) 081802 [arXiv:hep-ex/0411038].

[8] M. H. Ahn *et al.* [K2K Collaboration], "Measurement of neutrino oscillation by the K2K experiment", Phys. Rev. D **74** (2006) 072003 [arXiv:hep-ex/0606032].

[9] E. Church *et al.* [BooNe Collaboration], "A proposal for an experiment to measure muon-neutrino $\rightarrow$ electron-neutrino oscillations and muon-neutrino disappearance at the Fermilab Booster: BooNE", FERMILAB-PROPOSAL-0898.
A. A. Aguilar-Arevalo *et al.* [MiniBooNE Collaboration], arXiv:0704.1500 [hep-ex].

[10] A. A. Aguilar-Arevalo *et al.* [SciBooNE Collaboration], "Bringing the SciBar detector to the Booster neutrino beam", [arXiv:hep-ex/0601022].

[11] M. G. Catanesi *et al.*, [HARP Collaboration], "Measurement of the Production of charged Pions by Protons on a Tantalum Target", Eur. Phys. J. C **51** (2007) 787, arXiv:0706.1600 [hep-ex]

[12] M. G. Catanesi *et al.*, [HARP Collaboration], "Large-angle production of charged pions by 3 GeV/c–12 GeV/c protons on carbon, copper and tin targets", Eur. Phys. C **53** (2008) 177, arXiv:0709.3464 [hep-ex]

[13] M. G. Catanesi *et al.*, [HARP Collaboration], "Large-angle production of charged pions by 3 GeV/c–12.9 GeV/c protons on beryllium, aluminium and lead targets", Eur. Phys. C **54** (2008) 37, arXiv:0709.3458 [hep-ex]

[14] M. G. Catanesi *et al.*, [HARP Collaboration], "Large-angle production of charged pions with incident protons on nuclear targets as measured in the HARP experiment", submitted to Phys. ReV. C.

[15] M. G. Catanesi *et al.* [HARP Collaboration], "Measurement of the production cross-section of positive pions in p-Al collisions at 12.9 GeV/c", Nucl. Phys. B **732** (2006) 1 [arXiv:hep-ex/0510039].

[16] M. G. Catanesi *et al.* [HARP Collaboration], "Measurement of the production cross-section of positive pions in the collision of 8.9 GeV/c protons on beryllium", Eur. Phys. J. C **52** (2007) 29 [arXiv:hep-ex/0702024].

[17] M. G. Catanesi *et al.* [HARP Collaboration], " Measurement of the production cross-sections of $\pi^{\pm}$ in p-C and $\pi^{\pm}$-C interactions at 12 GeV/c", accepted for publication in Astroparticle Physics, DOI information: 10.1016/j.astropartphys.2008.02.002, arXiv:0802.0657 [astro-ph].

[18] W. F. Baker *et al.*, Phys. Rev. Lett. **7** (1961) 101.

[19] D. Dekkers *et al.*, Phys. Rev. **137** (1965) B962.

[20] J. V. Allaby *et al.*, CERN Yellow Report 70-12, 1970.

[21] Y. Cho *et al.*, Phys. Rev. D **4** (1971) 1967.

[22] T. Eichten *et al.*, Nucl. Phys. B **44** (1972) 333.

[23] D. Antreasyan *et al.*, Phys. Rev. D **19** N3 (1979) 764.

[24] I. Chemakin *et al.* [E910 collaboration] Phys. ReV. C **77** (2008) 015209.

[25] C. Alt *et al.* [NA49 Collaboration], Eur. Phys. J. C **49** (2007) 897 [arXiv:hep-ex/0606028].

[26] MIPP Collaboration, http://ppd.fnal.gov/experiments/2907/;
R. Raja, "The Main Injector particle production Experiment (MIPP) at Fermilab", Jour. Phys. Conf. Series **9** (2005) 303.

[27] N. Antoniou *et al.* [NA61 Collaboration], "Study of hadron production in hadron nucleus and nucleus nucleus collisions at the CERN SPS", CERN-SPSC-P-330, CERN-SPSC-2006-043, CERN-SPSC-2007-004, CERN-SPSC-2007-019.

[28] M. G. Catanesi *et al.* [HARP Collaboration], "The HARP Detector at the CERN PS", Nucl. Instrum. Meth. A **571** (2007) 527.

[29] M. Anfreville *et al.*, "The drift chambers of the NOMAD experiment", Nucl. Instrum. Meth. A **481** (2002) 339 [arXiv:hep-ex/0104012].

[30] M. Baldo-Ceolin *et al.*, "The Time-Of-Flight TOFW Detector Of The HARP Experiment: Construction And Performance", Nucl. Instrum. Meth. A **532** (2004) 548;
M. Bonesini *et al.*, "Construction of a Fast-laser Calibration System for the HARP TOF counter wall", IEEE Trans. Nucl. Science **50** (2003) 541.

[31] L. Durieu, A. Mueller and M. Martini, PAC-2001-TPAH142 *Presented at IEEE Particle Accelerator Conference (PAC2001), Chicago, Illinois, 18-22 Jun 2001*;
L. Durieu *et al.*, Proceedings of PAC'97, Vancouver, (1997);
L. Durieu, O. Fernando, CERN PS/PA Note 96-38.

[32] K. Pretzl *et al.*, Invited talk at the "International Symposium on Strangeness and Quark Matter", Crete, (1999) 230.

[33] M. G. Catanesi *et al.* [HARP Collaboration], "Particle identification algorithms for the HARP forward spectrometer", Nucl. Instrum. Meth. A **572** (2007) 899.

[34] G. D'Agostini, DESY 94-099, ISSN 0418-9833, 1994.
G. D'Agostini, Nucl. Instrum. Meth. A **362** (1995) 487.

[35] G. D. Barr *et al.* Phys. ReV. D74 (2006) 094009, astro-ph/0611266.

[36] Christine Meurer, "Muon production in extensive air showers and fixed target accelerator data", Ph.D. thesis, Karlsruhe, 2007, CERN-THESIS-2007-078.

[37] S. Agostinelli *et al.* [GEANT4 Collaboration], Nucl. Instrum. Meth. A **506** (2003) 250.

[38] A. Grossheim, "Particle production yields induced by multi-GeV protons on nuclear targets", Ph.D. thesis, University of Dortmund, Germany, 2003, CERN-THESIS-2004-010.

[39] J. R. Sanford and C. L. Wang, "Empirical formulas for particle production in p-Be collisions between 10 and 35 BeV/c", Brookhaven National Laboratory, AGS internal report (1967).

[40] D.H. Wright *et al.* AIP Conf. Proceedings 896 (2007) 11;
G. Folger and H.P. Wellisch, "String parton models in GEANT4 ", preprint CHEP-2003-M0MT007, e-print physics/0306007.

A Cross-section data

The tabulated cross-section data for p–C interactions at 12 GeV/c, already published in [17], are reported again here with a different binning for comparison.

Table 4: HARP results for the double-differential π^+ and π^- production cross-section in the laboratory system, $d^2\sigma^\pi/(dpd\Omega)$, for p–C interactions at 12 GeV/c. Each row refers to a different ($p_{\rm min} \le p < p_{\rm max}, \theta_{\rm min} \le \theta < \theta_{\rm max}$) bin, where p and θ are the pion momentum and polar angle, respectively. The central value as well as the square-root of the diagonal elements of the covariance matrix are given.

$\theta_{\rm min}$ (rad)	$\theta_{\rm max}$ (rad)	$p_{\rm min}$ (GeV/c)	$p_{\rm max}$ (GeV/c)	$d^2\sigma^{\pi^+}/(dpd\Omega)$ (mb/(GeV/c sr))	$d^2\sigma^{\pi^-}/(dpd\Omega)$ (mb/(GeV/c sr))
0.05	0.10	0.50	1.00	190.6 ± 27.1	132.3 ± 21.5
		1.00	1.50	237.3 ± 23.0	197.2 ± 20.9
		1.50	2.00	282.6 ± 23.2	189.6 ± 17.9
		2.00	2.50	266.1 ± 21.1	147.9 ± 14.8
		2.50	3.00	228.6 ± 18.1	102.2 ± 12.7
		3.00	3.50	166.6 ± 13.6	77.2 ± 9.1
		3.50	4.00	144.7 ± 13.7	55.7 ± 8.1
		4.00	5.00	83.6 ± 7.5	41.2 ± 5.0
		5.00	6.50	36.5 ± 4.2	8.6 ± 2.3
		6.50	8.00	16.4 ± 2.5	1.6 ± 0.9
0.10	0.15	0.50	1.00	209.9 ± 26.9	238.0 ± 32.3
		1.00	1.50	225.6 ± 23.1	207.0 ± 21.4
		1.50	2.00	264.1 ± 25.3	150.1 ± 16.5
		2.00	2.50	206.1 ± 20.4	94.9 ± 11.9
		2.50	3.00	135.4 ± 14.2	79.3 ± 10.4
		3.00	3.50	92.7 ± 10.5	50.2 ± 7.7
		3.50	4.00	60.5 ± 8.4	28.1 ± 4.4
		4.00	5.00	37.3 ± 4.7	17.2 ± 3.7
		5.00	6.50	9.5 ± 1.7	2.6 ± 0.9
		6.50	8.00	2.6 ± 0.7	0.2 ± 0.1
0.15	0.20	0.50	1.00	241.4 ± 31.7	223.5 ± 30.5
		1.00	1.50	213.2 ± 21.9	134.2 ± 17.2
		1.50	2.00	152.1 ± 16.8	128.7 ± 16.1
		2.00	2.50	90.8 ± 12.3	74.2 ± 11.0
		2.50	3.00	49.7 ± 8.4	51.1 ± 8.5
		3.00	3.50	31.3 ± 5.8	23.0 ± 4.8
		3.50	4.00	24.4 ± 5.2	11.3 ± 3.0
		4.00	5.00	11.3 ± 2.6	6.7 ± 2.0
		5.00	6.50	3.7 ± 1.4	0.5 ± 0.4
		6.50	8.00	0.6 ± 0.3	-
0.20	0.25	0.50	1.00	174.8 ± 26.6	146.1 ± 23.5
		1.00	1.50	80.7 ± 15.4	120.1 ± 19.4
		1.50	2.00	87.9 ± 17.3	108.4 ± 21.0
		2.00	2.50	44.2 ± 9.6	60.2 ± 13.7
		2.50	3.00	27.8 ± 7.7	24.5 ± 7.3
		3.00	3.50	18.0 ± 5.4	10.4 ± 3.8
		3.50	4.00	8.1 ± 3.5	4.9 ± 2.5
		4.00	5.00	5.1 ± 3.1	1.1 ± 1.3
		5.00	6.50	1.9 ± 1.4	-
		6.50	8.00	-	-

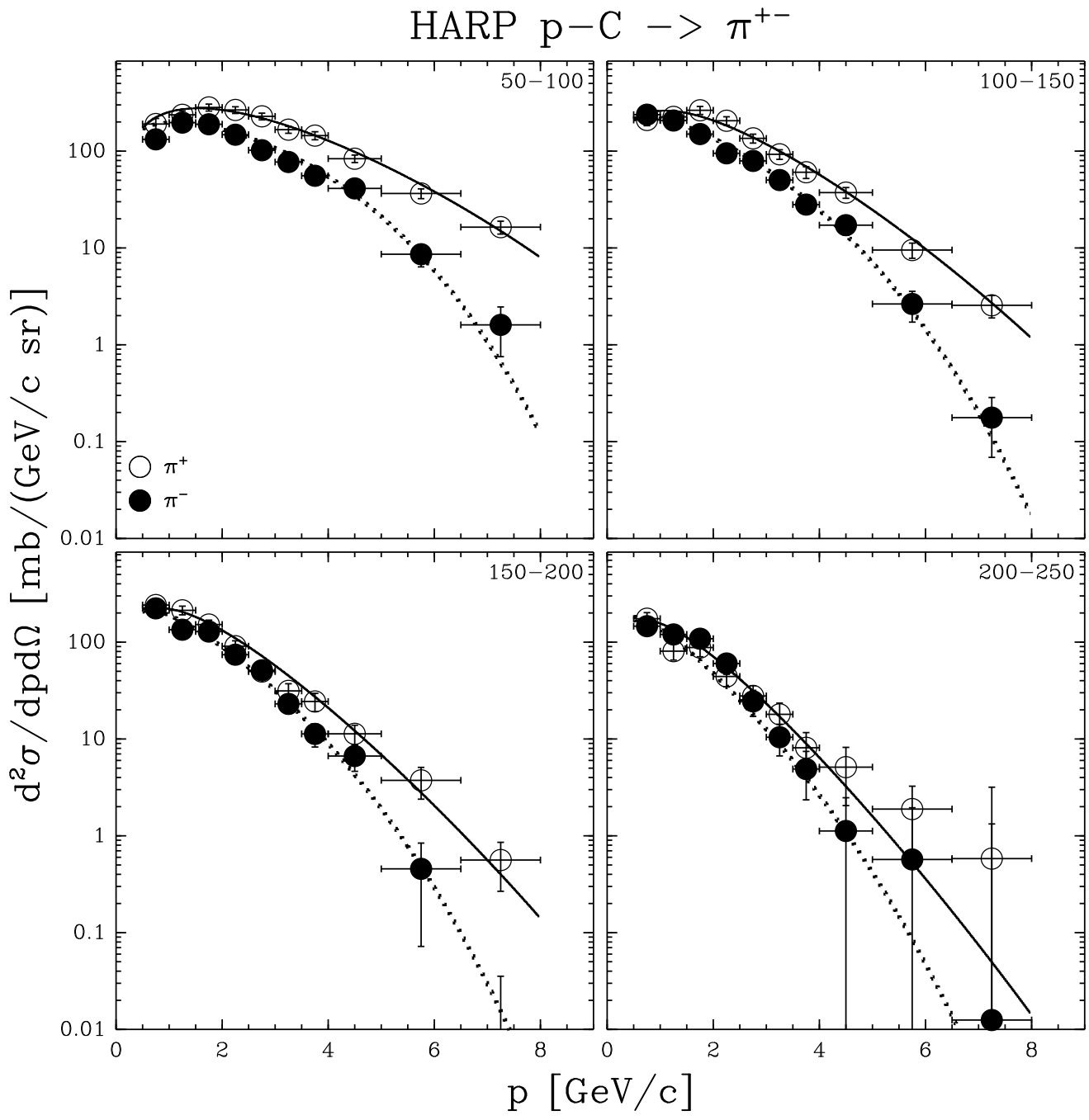
HARP p−C −> π+−
50−100
100−150
150−200
200−250
π+
π−
d²σ/dpdΩ [mb/(GeV/c sr)]
p [GeV/c]
0.01
0.1
1
10
100
0
2
4
6
8

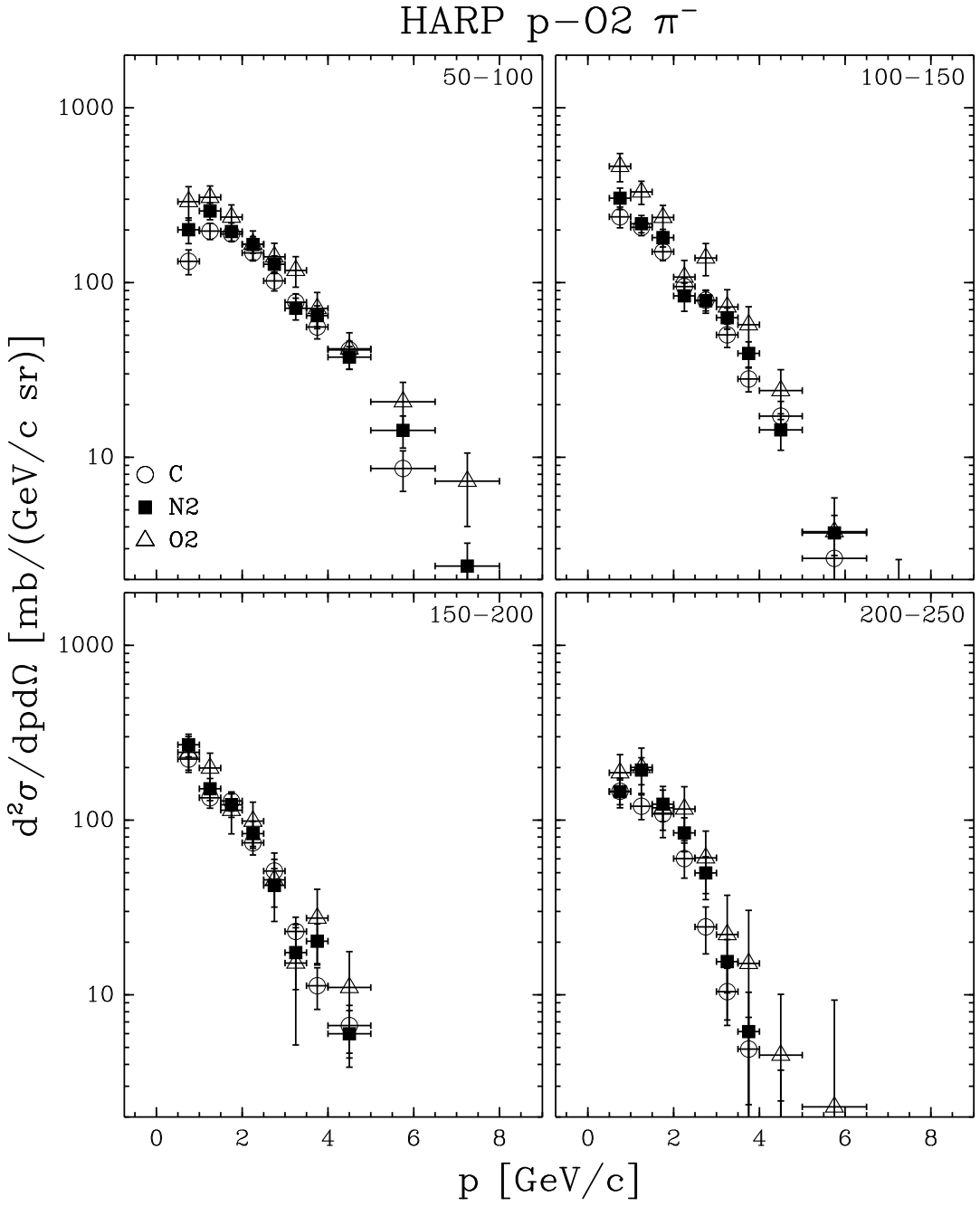
HARP p−O2 π⁻
50−100
100−150
150−200
200−250
C
N2
O2
1000
100
10
0
2
4
6
8
d²σ/dpdΩ [mb/(GeV/c sr)]
p [GeV/c]

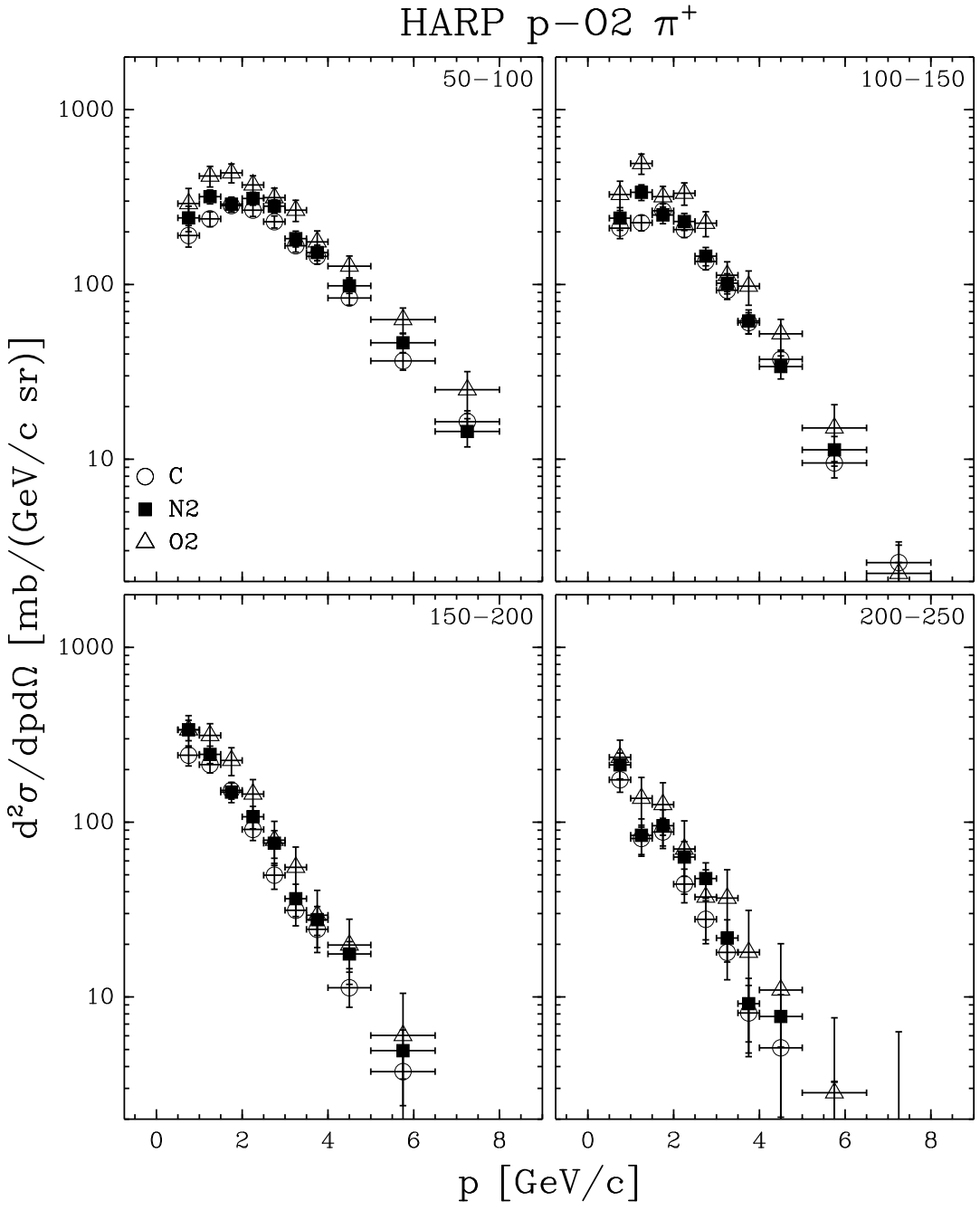
HARP p−O2 π+
50−100
100−150
150−200
200−250
C
N2
O2
1000
100
10
0
2
4
6
8
d²σ/dpdΩ [mb/(GeV/c sr)]
p [GeV/c]

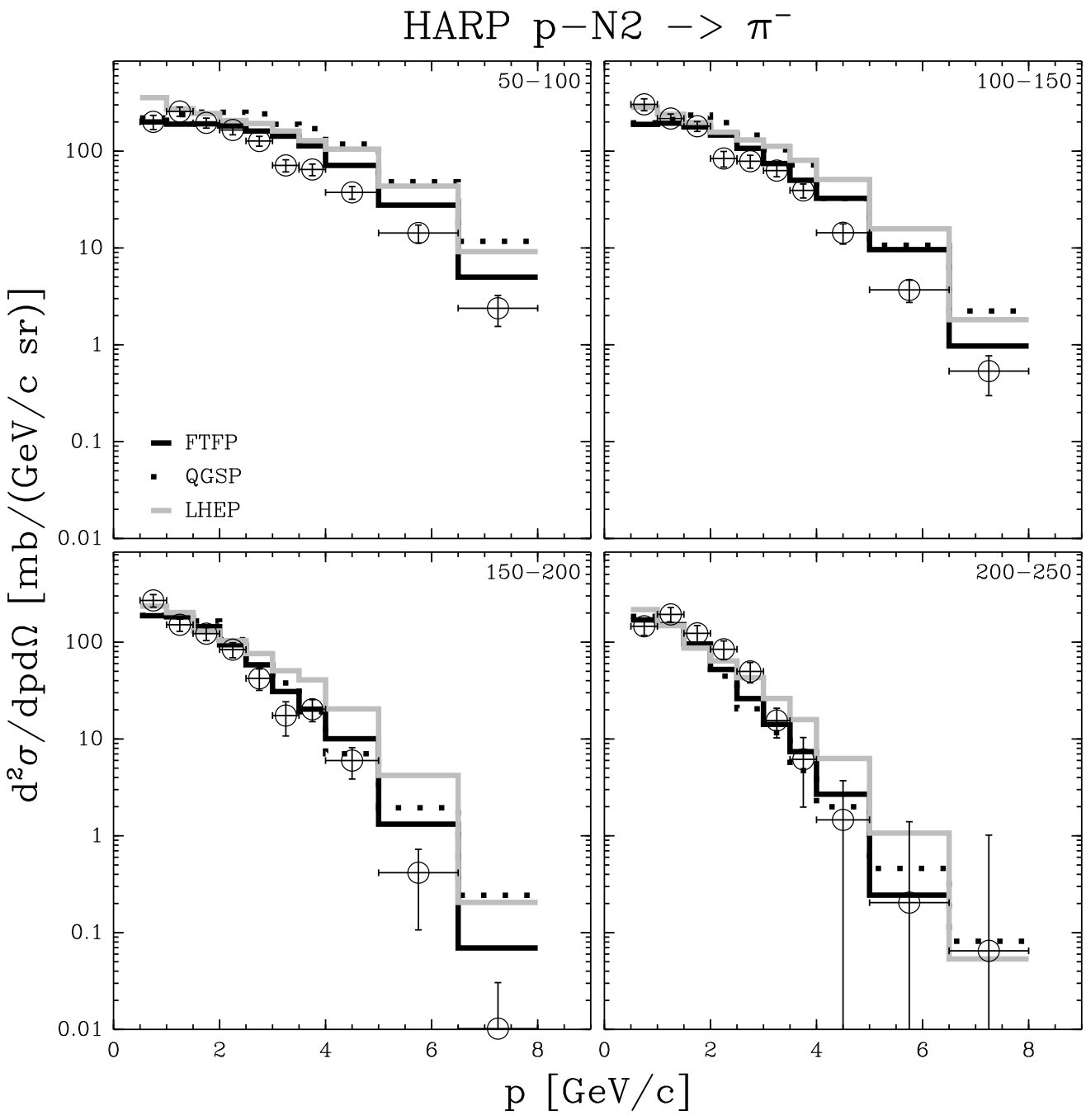
HARP p−N2 −> π⁻
50−100
100−150
150−200
200−250
FTFP
QGSP
LHEP
d²σ/dpdΩ [mb/(GeV/c sr)]
p [GeV/c]
0.01
0.1
1
10
100
0
2
4
6
8

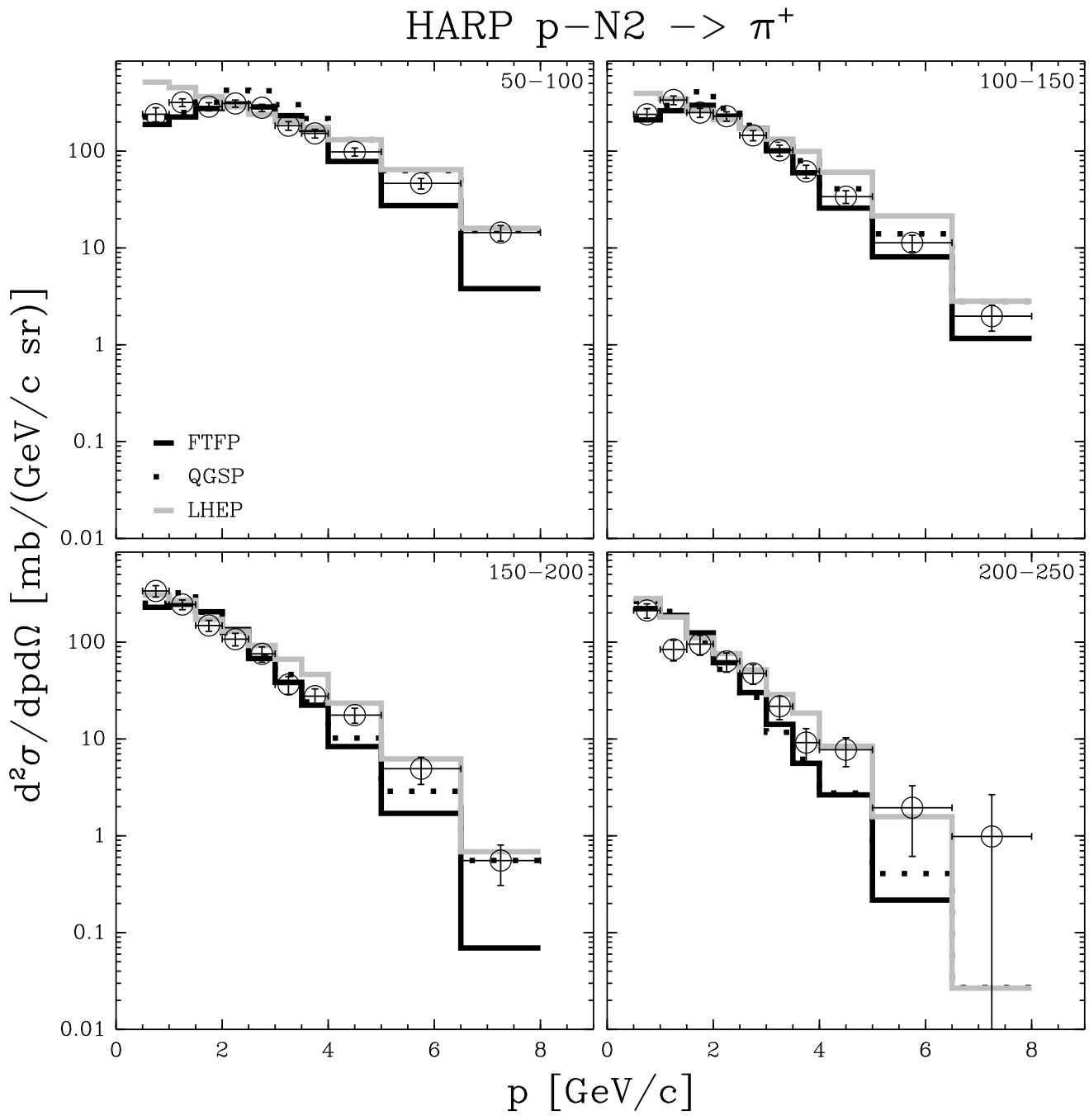
HARP p−N2 −> π+
50−100
100−150
150−200
200−250
FTFP
QGSP
LHEP
d²σ/dpdΩ [mb/(GeV/c sr)]
p [GeV/c]
0.01
0.1
1
10
100
0
2
4
6
8

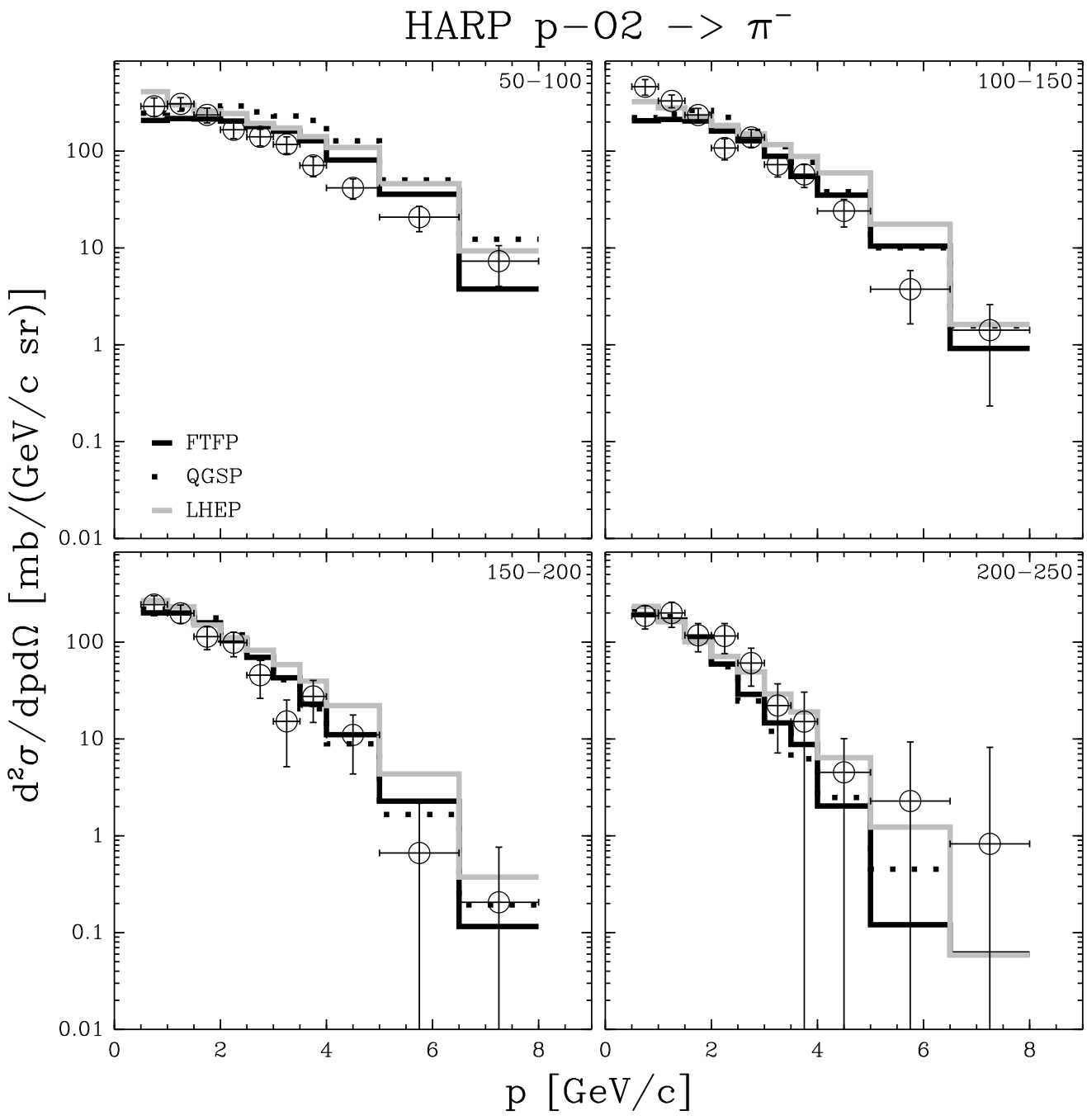
HARP p−02 −> π⁻
50−100
100−150
150−200
200−250
FTFP
QGSP
LHEP
d²σ/dpdΩ [mb/(GeV/c sr)]
p [GeV/c]
0.01
0.1
1
10
100
0
2
4
6
8

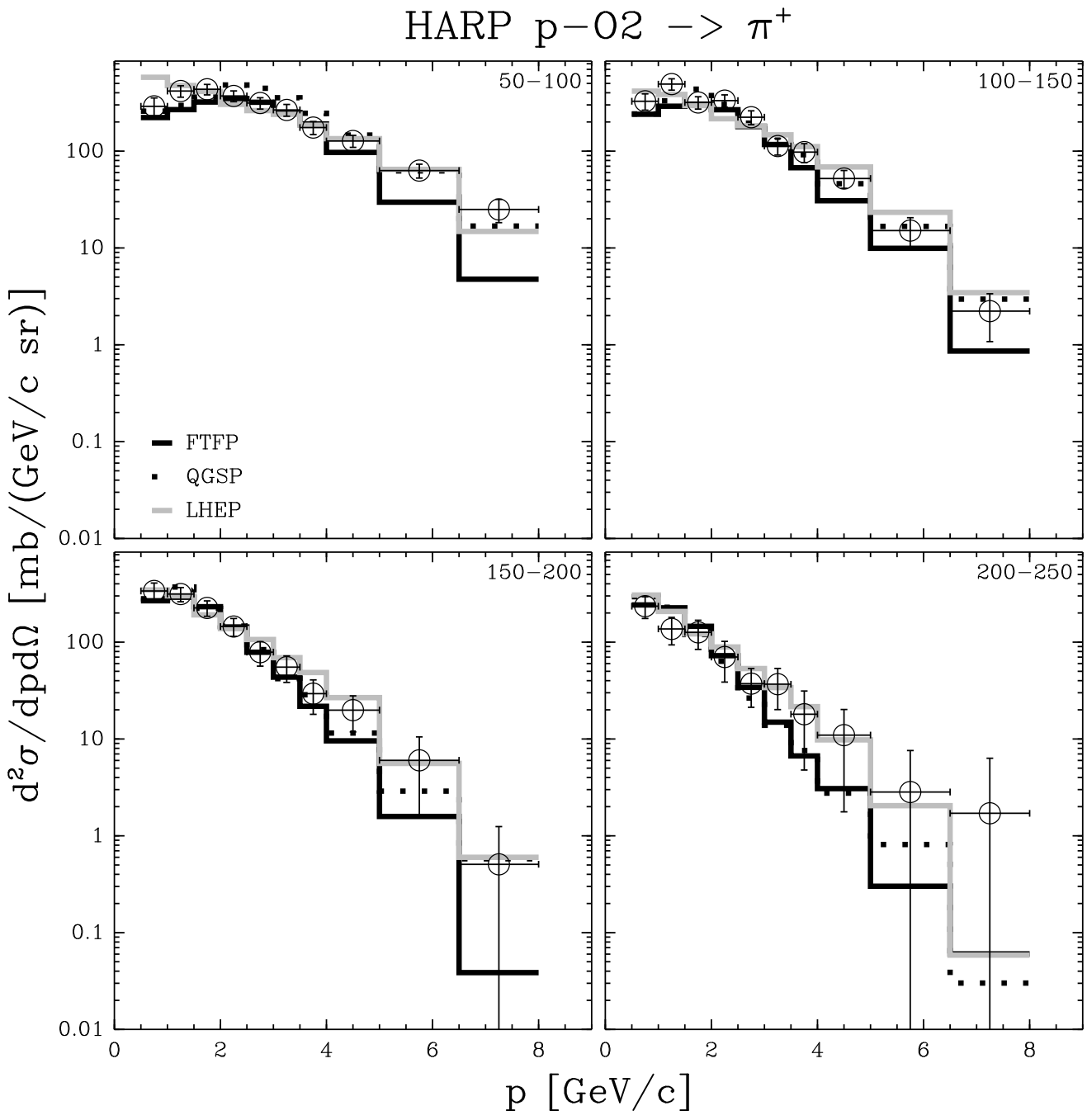
HARP p−02 −> π+
50−100
100−150
150−200
200−250
FTFP
QGSP
LHEP
d²σ/dpdΩ [mb/(GeV/c sr)]
p [GeV/c]
0.01
0.1
1
10
100
0
2
4
6
8

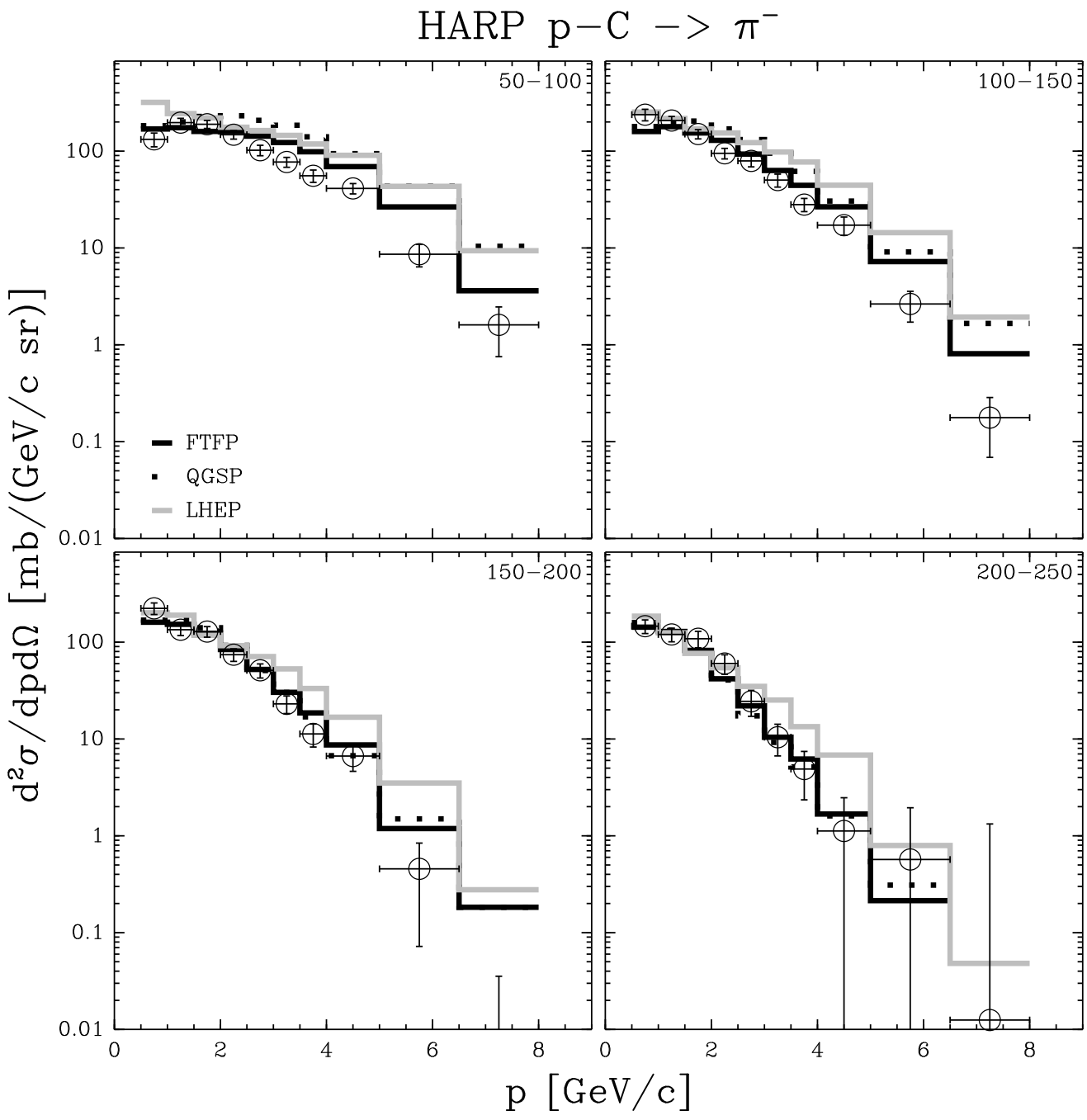
HARP p−C −> π⁻
50−100
100−150
150−200
200−250
FTFP
QGSP
LHEP
d²σ/dpdΩ [mb/(GeV/c sr)]
p [GeV/c]
0.01
0.1
1
10
100
0
2
4
6
8

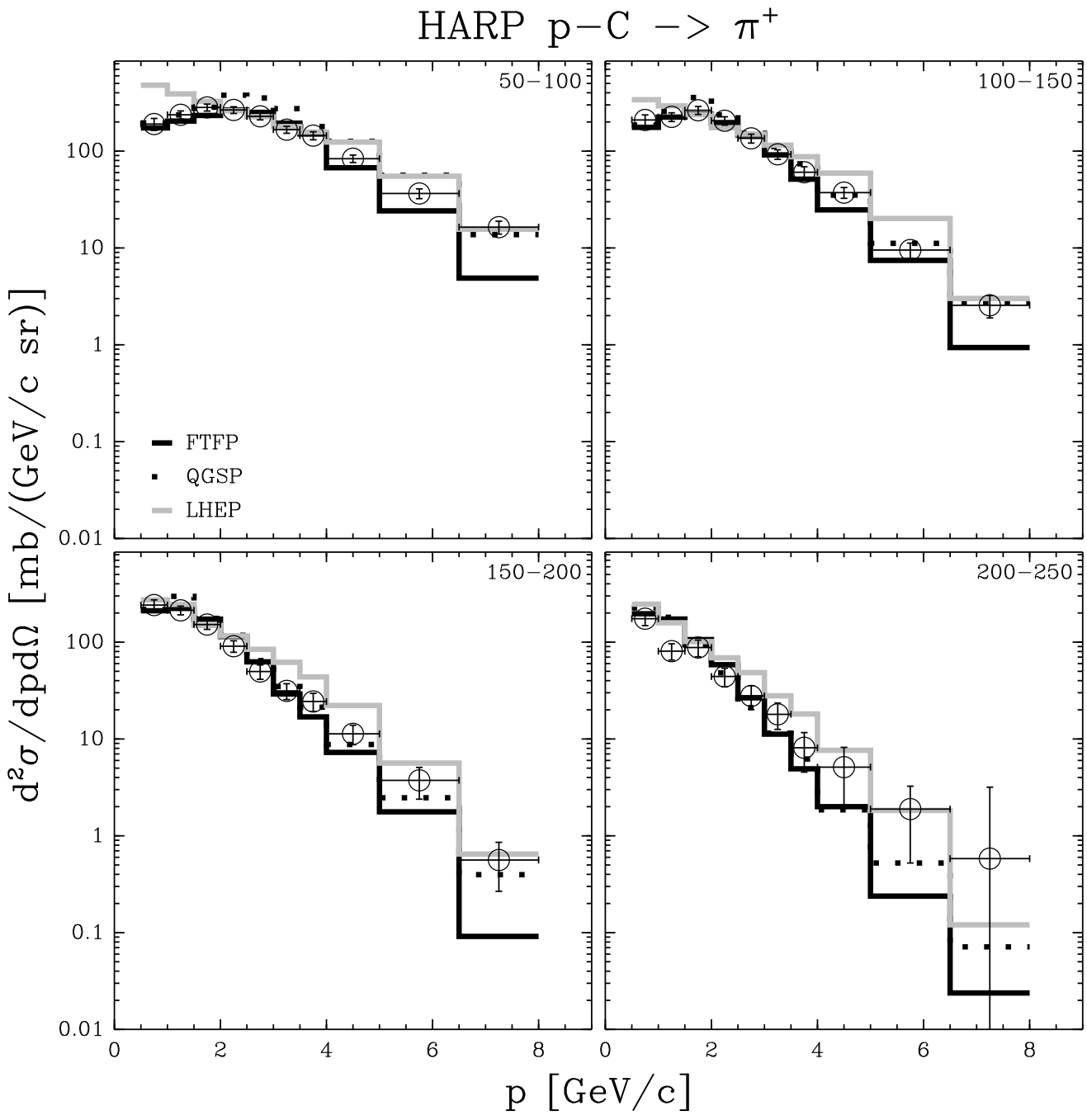
HARP p−C −> π+
50−100
100−150
150−200
200−250
FTFP
QGSP
LHEP
d²σ/dpdΩ [mb/(GeV/c sr)]
p [GeV/c]
0.01
0.1
1
10
100
0
2
4
6
8

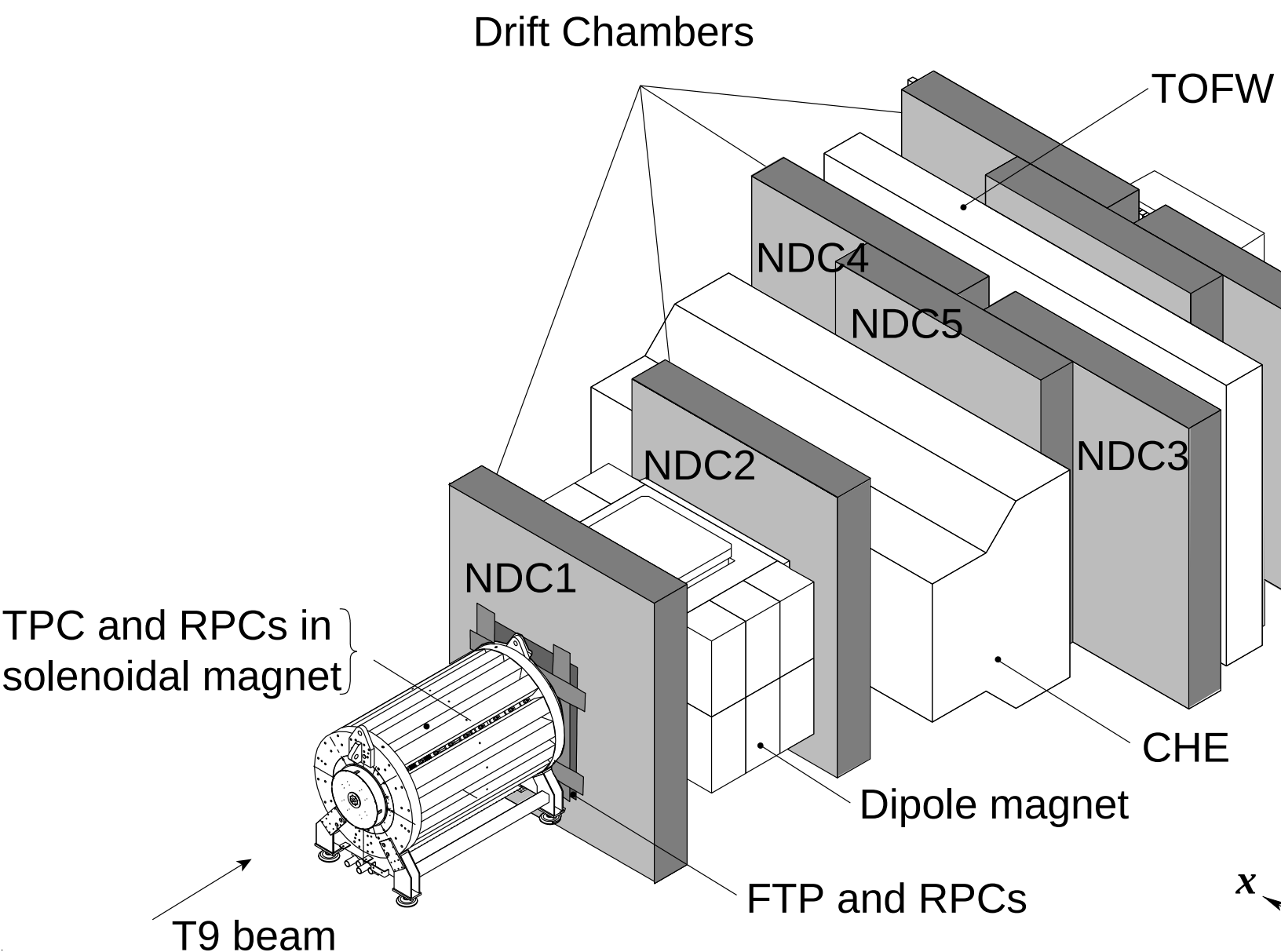
Drift Chambers
TOFW
NDC4
NDC5
NDC3
NDC2
NDC1
TPC and RPCs in
solenoidal magnet
CHE
Dipole magnet
FTP and RPCs
T9 beam
x